heritage

MDPI

Article

Revealing the Materials, Painting Techniques, and State of Preservation of a Heavily Altered Early 19th Century Greek Icon through MA-XRF

Georgios P. Mastrotheodoros *, Anastasios Asvestas, Theofanis Gerodimos and Dimitrios F. Anagnostopoulos

Department of Materials Science and Engineering, University of Ioannina, GR 45110 Ioannina, Greece
* Correspondence: gmastrotheod@uniwa.gr

Abstract: Macroscopic X-ray fluorescence analysis (MA-XRF) is a non-destructive analytical technique that allows for the rapid and thorough investigation of paintings; therefore, it is nowadays increasingly involved in relevant studies. In the present work, a state-of-the-art MA-XRF set-up is utilized to identify the painting materials and techniques and document the state of preservation of an early 19th-century AD Greek religious panel painting ("icon"). The artifact in consideration has received extensive restoration interventions in the past and is considerably decayed; for these reasons, the interpretation of the relevant MA-XRF elemental intensity distribution maps is challenging. In this framework, it is demonstrated how the elemental distribution maps can be explored and interpreted to lead to a thorough investigation of the painting in consideration. In particular, the MA-XRF data interpretation allowed for the identification of the original palette that includes the rather rarely employed–in icon painting-yellow lead-antimonate pigment, led to the spotting of an invisible inscription, to the documentation of the preparation/gesso layer and the preliminary drawing. Additionally, it was possible to discriminate between the original painting and the later interventions, while the collected data revealed that the painting originally had two cross-bars attached to its back. Ultimately, the presented case study can be utilized as a guide for the proper interpretation of MA-XRF data from decayed and altered icons.

Keywords: macro X-ray fluorescence imaging; elemental maps; Compton scattering; pigment; gilding; conservation; restoration

Citation: Mastrotheodoros, G.P.; Asvestas, A.; Gerodimos, T.; Anagnostopoulos, D.F. Revealing the Materials, Painting Techniques, and State of Preservation of a Heavily Altered Early 19th Century Greek Icon through MA-XRF. *Heritage* **2023**, *6*, 1903–1920. https://doi.org/10.3390/heritage6020102

Academic Editors: Valeria Di Tullio and Brenda Doherty

Received: 31 December 2022
Revised: 9 February 2023
Accepted: 9 February 2023
Published: 13 February 2023

1. Introduction

X-ray fluorescence spectroscopy (XRF) has found wide application in the investigation of tangible cultural heritage items because it allows for a rapid, accurate, and absolutely non-invasive elemental characterization [1]. Moreover, X-rays penetrate significantly deeper into the matter compared to visible light photons; therefore, XRF analysis may often extract information that pertains not only to the (visible) surface but to the invisible substrate(s) as well. In case of paintings, the radiation penetration depth depends on various factors such as the paint layer composition, the radiation photon energy, incident photon direction, etc. [2]; however, X-rays penetrate significantly deeper into paint layers (up to tens of microns) in comparison to visible light photons (nanometers) (see Section 3.2.1.

Advances in the field have led to the development of macroscopic XRF setups (MA-XRF) that are able to collect and process multiple successive spectra in a pre-defined x–y matrix; based on this data, one may extract the intensities of particular elemental peaks and plot them in 2-D element distribution maps. The 2-D graphic representation of elemental distributions can be utilized as an extremely powerful tool for extracting information pertaining to the materials and manufacturing techniques of the studied artifacts, for MA-XRF analysis has found wide application in the field of paintings' investigation. Besides, MA-XRF allows us to detect the elemental profile in areas at high spatial resolution (for a macroscopic technique) and to plot the local distribution of individual elements, depending

on their cross-section and stratigraphy of application. On this basis, it is apparent that MA-XRF offers invaluable data that, although they may not lead to a straightforward identification of a given inorganic component, do provide strong hints as to the nature of the employed compounds. Therefore, numerous studies have included MA-XRF in order to retrieve information about pigments and other painting materials, as well as to document previous interventions and the state of preservation of old paintings and relevant artifacts [3–15]. However, despite the rather wide application of this technique in the analysis of paintings, there exist only a couple of published MA-XRF studies of post-Byzantine portable icons (i.e., post-1453 A.D. Eastern Orthodox Christian religious panel paintings) [6,16]. Additionally, most of the post-Byzantine icons have been manufactured by employing a rather standardized technique [17–20]; therefore, through the meticulous interpretation of MA-XRF data, one can retrieve extremely valuable data pertaining to icons' painting materials and techniques, as well as to their state of preservation.

Here, it shall be noted that the practice of icon painting is a very old tradition; in fact, it is thought to have emerged shortly after the birth of Christianity, and one view relates its infancy to the contemporary tradition of Egyptian funerary portraits [21]. Note, however, that although in terms of materials and techniques–and to some extent style too-icons certainly share a common background with some funerary portraits [22], it appears that they represent a distinct artistic creation [23]. In any case, it seems that icon painting was established after the declaration of Christianity as the official religion in Roman Empire (380 A.D., Emperor Theodosius I) and was gradually spread in most of the territories where Christians lived. Indeed, icon painting was practiced in a vast area spanning from Egypt and Ethiopia to Russia, as well as from Italy to Asia Minor and the region of Caucasus [21,24].

Interestingly, in the region of modern-day Greece, icons are continuously manufactured during at least the last fifteen centuries, a time framework that includes a prolonged period of conquest by the Ottoman Turks (~1450–1830 AD), the so-called post-Byzantine period [25]. From the perspective of their materiality, icons have been persistently manufactured by following (occasionally slightly modified) versions of medieval painting techniques, i.e., they were painted on gessoed wooden panels by using egg yolk tempera, they incorporated gilded decorations, etc. [17–20,26,27]. Note that the persistent use of traditional materials and techniques shall be considered in comparison to the contemporary trends of Western European painting, where painters gradually abandoned medieval practices and adopted oil painting on fabric supports.

Being veneration objects that played a major role in the everyday ritual life of Orthodox Christians, icons were often subjected to decay and alterations. Therefore, it was a common practice to treat them in order to restore their integrity. Such treatments were often limited to overpainting, yet in some instances, craftsmen were performing substantially more complex interventions, including the impregnation of rotten panels with glue ("consolidation"), the removal of surface contamination and oxidized varnishes using alkaline or alcoholic solutions ("cleaning"), the integration of gesso and paint losses ("retouching"), regilding, etc. In fact, recipes dictating such practices are included in several 18th- and 19th-century Greek painting manuals, and most of them include warnings of the potential dangers of careless application of the described practices [28]. Unfortunately, interventions of this type were often executed by non-specialized craftsmen and without taking the needed precautions, often thus resulting in severe alteration/losses of the original painting, commonly treated by overpainting.

Icons that have passed through (often multiple) older interventions are occasionally the subject of modern analytical investigations that aim at distinguishing the original from the latter elements. Due to complexity, this type of investigation often requires sampling and samples cross-section analysis. However, collecting samples from antique paintings/veneration objects is not always possible, and in such cases, extracting the desired information through non-invasive analytical protocols is imperative.

In the current work, authors demonstrate the potentialities of MA-XRF analysis through the investigation of a heavily altered early 19th-century icon, i.e., a Greek Orthodox Christian religious panel painting (Figure 1). This artifact was selected as an ideal case study because it has undergone severe decay resulting in extensive paint and gesso losses and has received extensive later interventions; through MA-XRF analysis authors aimed to resolve issues pertaining to the distinction between the authentic elements and later interventions. Moreover, the rather small dimensions of the artifact allowed for its handy manipulation in the framework of laboratory analysis, while its very rare iconographic theme (see next) was inspiring as well. Apart from MA-XRF, and in order to further exploit technological features, the painting was also examined by X-ray radiography (XRR), a method very commonly employed in the field of painting investigation [29,30].

Figure 1. The recto and verso of the studied icon (left and right respectively).

The artifact in consideration belongs to a private collection and depicts two saints, namely St. John the Forerunner on the left and a Hierarch on the right (Figure 1). The painting is severely altered and bears no signature or other elements revealing its authorship. However, it does show stylistic features that are reminiscent of those seen on contemporary icons that originate from Western Greece and the Ionian Islands, therefore a relevant provenance seems probable. A characteristic example is the posture of St. John, whose right hand is extended towards the right in a blessing gesture, whilst his head is slightly inclined and turned towards the opposite direction (Figure 1). This posture is more vivid in comparison to the typical, rather stiff post-Byzantine representations of St John the Forerunner (see e.g., icons 233 in [31], 6 in [32], 9 in [33] and several examples in [21,34]). Note also that, although in the framework of Greek religious painting there do exist several icons that depict St John either alone or as part of larger syntheses (see for instance the iconographic type of "Deesis" where St John is portrayed with Jesus Christ and the Virgin Mary, e.g. icons, 11 and 105 in [33] and 55 and 116 in [34]), it is very uncommon to spot icons representing St John in full length standing next to another Saint. A relevant example is an 18th-century icon of St John and St Nikolaos that presumably originates from Greek islands and is kept in a Swiss private collection [32]. Art historians have claimed that such icons reflect patrons' preferences, who occasionally asked painters to depict specific saints in the icons they ordered (see e.g., icons 41 in [32] and 143 in [34]); the relevant items were often meant to be used for private worship [32]. On this basis, it is assumed that

the icon in consideration was produced in the same framework, and its rather small size (18.2 × 13.5 cm^2) corroborates the assumption that it was worshiped in private.

2. Materials and Methods

For the purposes of the current study, an early 19th-century Greek icon was investigated. The studied artifact measures 18.2 × 13.5 × 2.0 cm^3 (height × width × thickness) and depicts Saint John the forerunner and a Hierarch, both in full length standing on greenish ground (Figure 1, left). The icon was preliminarily investigated through spot XRF analysis conducted by using a milliprobe XRF spectrometer and, subsequently, macro-XRF (MA-XRF) and X-ray radiography (XRR); additionally, the artifact was examined and photographed through a stereoscope.

2.1. Spot XRF

The milliprobe XRF spectrometer (spot size: ~2.5 mm^2) is equipped with an Rh-anode X-ray tube (50 W, 50 kV, 75 μm Be window) and a Si-PiN detector (XR-100CR, Amptek Inc., Bedford, MA, USA) with a 500-μm nominal crystal thickness (resolution: 165 eV FWHM at Mn Kα). Several spots on the icon were examined by using the aforementioned spectrometer operating in a 40 kV voltage and varying current (90–120 μA, adapted to achieve high count rate).

2.2. MA-XRF

The MA-XRF analysis of the icon was conducted by using the M6-Jetstream scanner (Bruker Nano GmbH, Berlin, Germany), which is equipped with a 30 W Rhodium anode X-ray tube (maximum high voltage: 50 kV) with polycapillary optics and a silicon drift detector (active area: 30 mm^2). The polycapillary full lens focuses the emitted X-ray radiation from the tube on the target. From the initial power of 30 W, the estimated radiation power hitting the target is about 10 μW [35]. For the analysis of the icon's recto (painting), the X-ray tube was operated in a voltage and current setting of 50 kV and 600 μA, respectively. The beam spot size was set to a diameter of 100 μm and the scanning step/pixel size to 200 μm (no filter), while the dwell time was set to 20 ms. These parameters resulted in an overall scanning time of 4 h and 8 min and in collecting 612,000 individual spectra from the painted area. For scanning the wooden support sides and verso, the X-ray beam spot size was again set to 100 μm and the scanning step/pixel size to 300 μm (dwell time: 10 ms). In all the cases, the collected spectra were processed and visualized (i.e., transformed into elemental distribution maps) using the built-in M6-Jetstream software.

2.3. XRR

For the X-ray radiography, a Polydoros SX 50 (Siemens, equipped with an Opti 150/30/50/C X-ray tube) generator was used in 40 kVp and 3 mAs conditions during the irradiation of the icon; a single radiograph was acquired, and the resolution of the corresponding image was 1524 × 2032 pixels. The digital radiograph was processed using the DIRECTVIEW CR Elite (Kodak, New York, NY, USA) system.

2.4. Stereoscope

Details of the icon were examined and photographed by attaching a digital camera on the eyepiece of a Leica Wild M3B stereoscope able to provide magnifications of 6.4×, 16× and 40× (with field of view values equal to 27.5 mm, 9.8 mm, and 4.8 mm, respectively).

3. Results and Discussion

3.1. Preliminary Considerations

Prior to creating the elemental intensity maps, the elements were detected on the MA-XRF sum spectrum (i.e., the sum of the individual spectra collected during the scan) and the maximum pixel spectrum (the maximum pixel spectrum is constructed by selecting the maximum pixel intensity value within each X-ray energy channel, ignoring the remaining

pixels). For example, in the case of the icon's recto, the detected elements include Si, P, S, K, Ca, Ti, Ba, Cr, Mn, Fe, Cu, Zn, Au, Hg, and Pb (Figure 2, left-(a)). However, particular attention should be paid to detecting minor or trace elements. Their detection is highly challenging if their characteristic energies are in energy regions where the spectrometer's detection efficiency is low and/or superimposed with high-intensity spectral lines of major elements. A characteristic example that emerged during the current study concerns the detection of Sb. The Sb Kα transition energy at 26.4 keV corresponds to an energy region at which the M6-Jetstream spectrometer's detection efficiency is very low. Moreover, the Sb Lα transition line at 3.605 keV overlaps with the high intensity of Ca Kα transitions at 3.691 keV. Consequently, in the case of Sb traces in a small number of pixels, its detection is a highly complex task without preliminary information for its appearance, as the Sb characteristic lines are not observed either at the sum (Figure 2, left-(a)) or at the maximum pixel spectra. On this basis, it is evident that this element might have gone unnoticed if not for its detection during the preliminary spot milliprobe XRF analysis (Figure 2, left-(b)). Note, however, that the existence of Sb can also be revealed solely on the basis of the M6 XRF data, through the examination of sum spectra from the corresponding areas of the work. In particular, Figure 2 (middle) shows the sum XRF spectrum of the whole icon versus the spectra from the left wing and the book cover in the energy range of the Ca K X-rays; the spectra were normalized to the peak position of the Ca Kα (3.691 keV). In the sum spectrum of the whole icon, the Sb Lα (3.605 keV) and Lβ (3.843 keV) transitions are not distinguished. However, in the case of the wing and book cover areas, the Sb Lα appears clearly as broadening on the low energy side of the Ca Kα, while the Sb Lβ creates a bump between the Ca Kα and Kβ transitions. Consequently, the Sb L transitions can be separated from the Ca K transitions in the wing and the book cover areas. This elaborate analysis leads to the Sb spatial detection in the yellowish highlights of St John's wings, the book's cover held by the Hierarch, and part of the greenish ground (Figure 2, right). This case highlights the need to perform a careful and assiduous evaluation of the MA-XRF data while searching for the presence of elements in the sum and maximum pixel spectra.

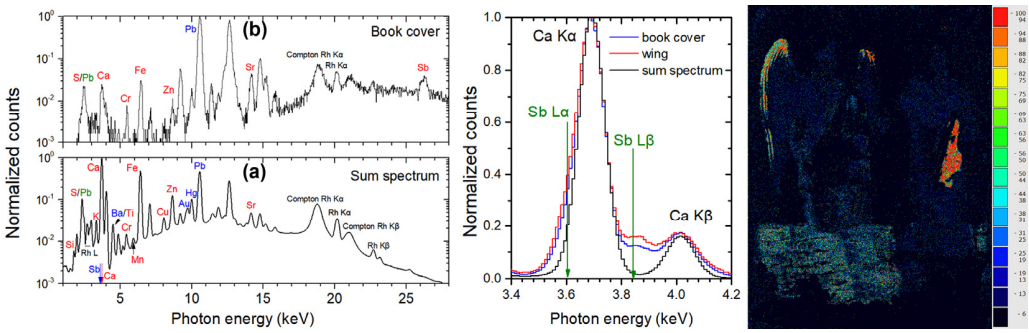

Figure 2. (**Left**) MA-XRF sum spectrum, icon's recto (**a**) and milliprobe XRF spectrum collected from the Hierarch's book cover (**b**). Middle: Details of the MA-XRF spectra collected from the Sb-bearing areas (St John's wing and Hierarch's book) versus the sum spectrum. (**Right**) elemental distribution map of Sb (Lβ) created in the framework of MA-XRF analysis.

Additionally, another critical parameter in deciding upon the creation of elemental distribution maps is whether the maps will be displayed in grayscale or in color. Although the former option is adopted by most scholars working in the field (see, e.g., [5,8,9]), the current authors opt for the latter [16]. Besides, by using an RGB scale that ranges from black (zero counts) through selected tones of blue and light blue (50% of maximum intensity/counts) to yellow and hot red (maximum intensity/counts), one can more precisely reveal slight variations in elemental peak intensities. A characteristic example is shown in Figure 3, where the Pb elemental distribution map of the bottom side of the icon in grayscale and RGB is demonstrated. Comparing the corresponding maps shows that some areas appear uniform in intensity in the grayscale map yet show considerable variation when displayed in RGB. For this reason, the RGB mode will be used throughout the current work.

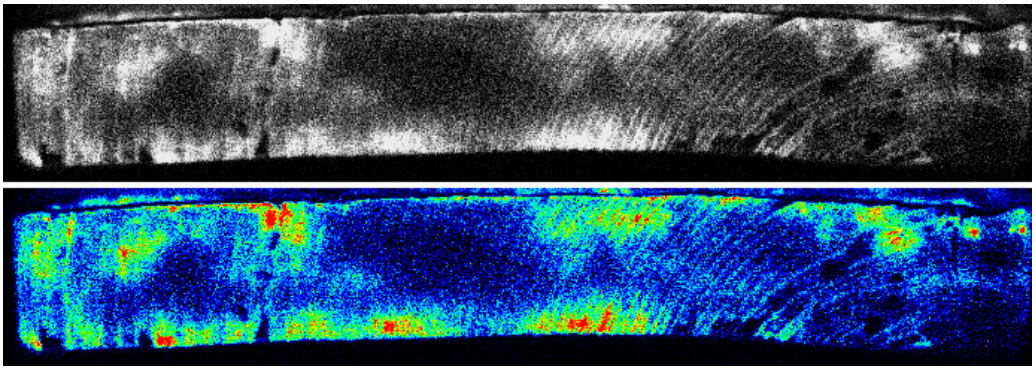

Figure 3. Bottom side of the icon: the elemental distribution map of lead (Pb-Lα) in grayscale (**up**) and in RGB (**bottom**).

3.2. The Recto of the Icon (Painting)

For reasons of convenience, the presentation of the complex MA-XRF data that pertain to the recto of the icon is presented following a "stratigraphic" sequence, i.e., the data that relate to the substrate/ground of the painting are presented first and then follow the presentation of the data that pertain to the gilding and the paint layers.

3.2.1. The Ground/Preparatory Layer

Ca is detected in a major part of the icon but appears intensified in areas where paint layers have been lost, revealing the painting substrate, such as, for example, the background between the two Saints and the lower part of the artifact (Figure 4). Moreover, the intensity of Ca is inversely related to the intensities of various pigment-related elements, such as Fe, Au, Pb and Hg, as Ca faints where these elements show up (see e.g., Figure 4). The latter is due to the rather low energy of the Ca Kα photons (3.68 keV) that are attenuated by the paint layers containing high-Z elements. An indicative diagram of the penetration depth as a function of the photon energy in selective painting materials is shown in Figure 5 [36]. On this basis, it is concluded that Ca is primarily associated with the painting substrate, namely the gesso/preparatory ground layer that is almost always applied on the wooden panel prior to painting in the framework of post-Byzantine iconography [18,20]. It is worth noting that the primary purpose of the ground is to provide a homogeneous—in terms of both texture and properties (absorbance, texture, and color)—layer that is adequate for painting; in other words, the ground is applied in order to overcome the adverse effect(s) of wood grain/texture on the properties of the wooden substrate. In the current case, most of the Ca appears strongly related to S (Figure 4), thus indicating the employment of a calcium sulfate compound in the ground; such compounds were very commonly used in southern Europe, while calcium carbonate was far more popular in central and northern European painting [18,37]. Interestingly, the lower part of the icon shows very intense Ca elemental peaks yet no S, highlighting thus that there has been employed a calcium carbonate compound to compensate for the extensive gesso losses in this area (Ca map, Figure 4). Finally, it is noted that Sr (Figure 4) is distributed relatively homogenously on the painting but in the area of the later filler on the lower part of the icon and the areas where high-Z elements, such as Pb and Hg, show high intensities (Figure 6). Note that the mean penetration depth for the Sr Kα transition photons (14.17 keV) is more than 10 microns in paint layers that contain lead white (Pb) or cinnabar (Hg) (Figure 5). On this basis, it is inferred that Sr pertains primarily to the original ground layer (Ca-S compound), and presumably reflects the presence of minor celestine (strontium sulfate), a mineral associated with calcium sulfate compounds and often spotted as a minor admixture in the grounds of post-Byzantine icons and other paintings [18,38].

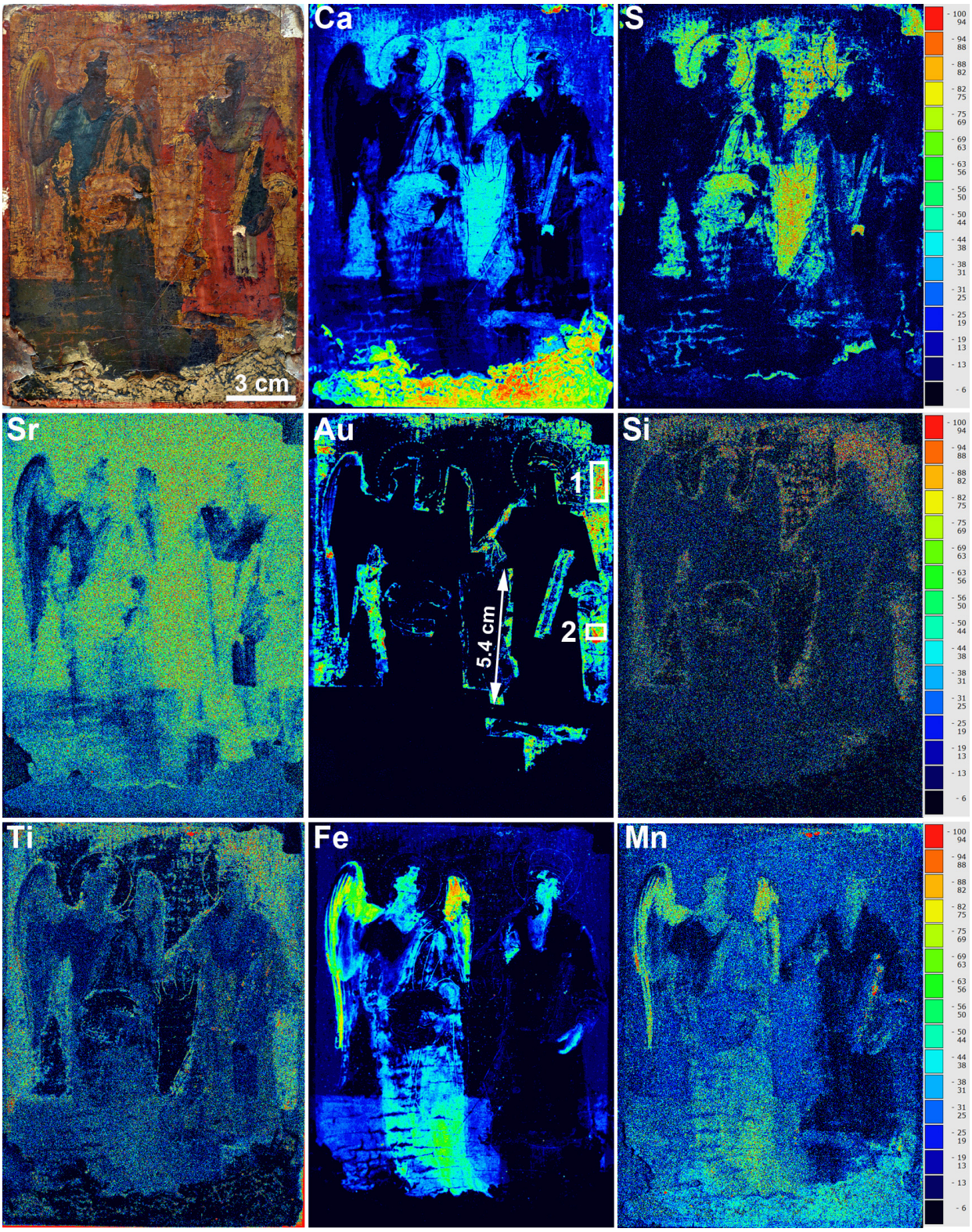

Figure 4. From upper left to bottom right: a photograph of the studied icon and the elemental distribution maps of Ca (Kα), S (Kα), Sr (Kα), Au (Lα), Si (Kα), Ti (Kα), Fe (Kα), and Mn (Kα). Elemental peak intensities are represented in a multicolor scale (pixels with the maximum intensity for a given elemental peak are colored red, while blackish pixels correspond to zero counts). On the Au map, the maximum observable gold leaf width is marked with an arrow.

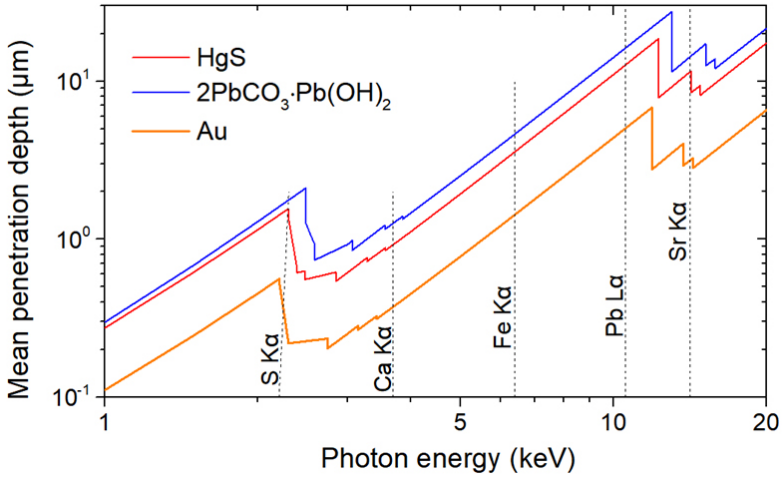

Figure 5. Evaluated mean photon penetration depth for cinnabar (HgS), hydrocerussite ($2PbCO_3 \cdot Pb(OH)_2$), and Gold (Au) as a function of the photon energy [36]. The energy position of specific X-ray characteristic transitions is shown.

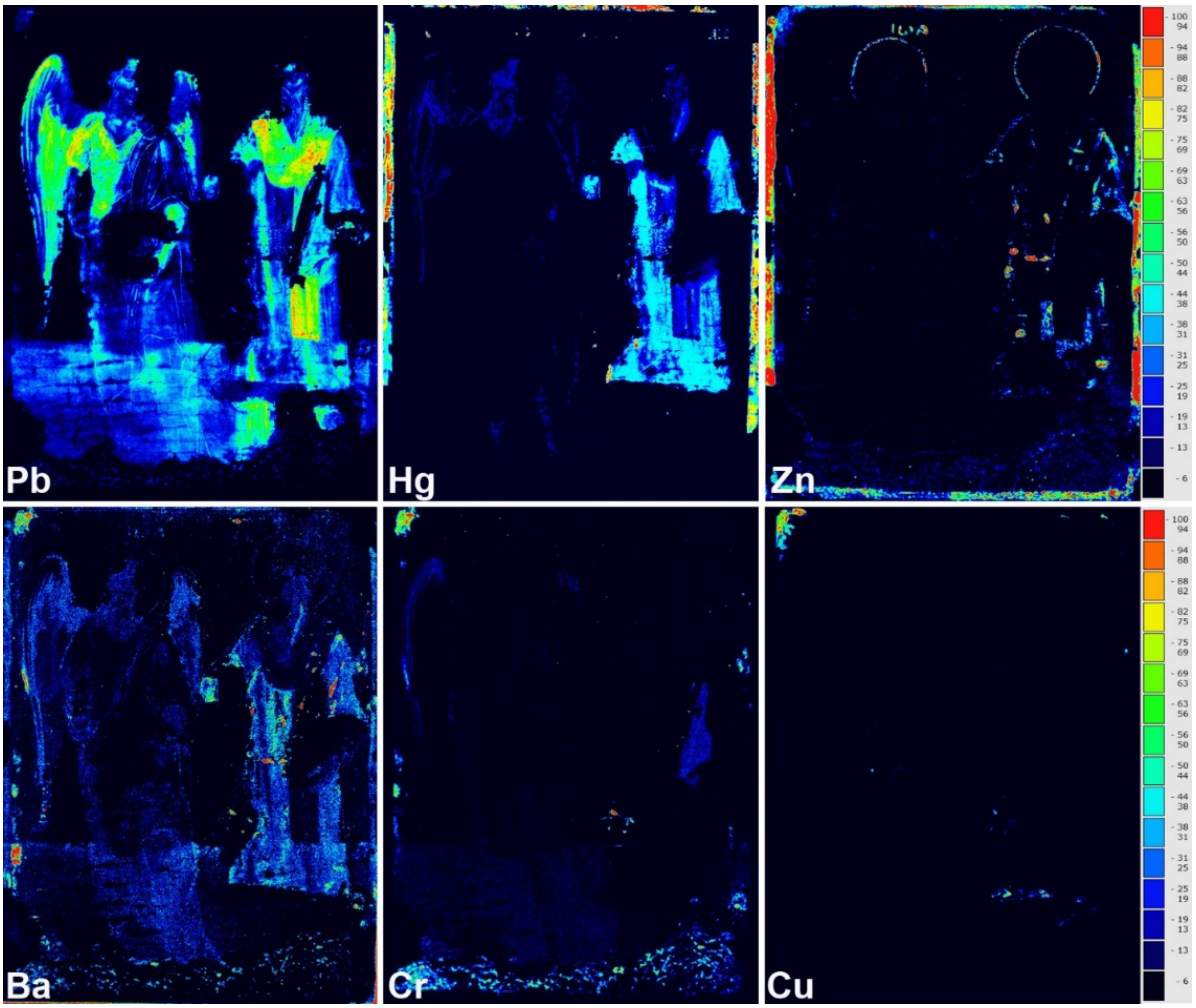

Figure 6. From upper left to bottom right: elemental distribution maps of Pb (Lα), Hg (Lα), Zn (Kα), Cu (Kα), Cr (Kα), and Ba (Lα).

3.2.2. The Gilded Decorations

Au is detected on the gilded campus/background of the painting and elsewhere, such as in details of the vestment and the spine of the book kept by the Hierarch. The corresponding MA-XRF elemental distribution map is shown in Figure 4 and reveals the extensive losses of the gold leaves from the icon's background. In order to determine the composition of the employed gold leaves, the sum spectra of two defined rectangular areas on them ("1" and "2" on the Au map, Figure 4) were thoroughly studied. Except for the Au L X-ray transitions, the Cu K transition was observed in both spectra, while Ag K or L transitions were not detected. The intensity ratio of the Cu Kα to the Au Lα was 11.4% and 11.7% for the areas "1" and "2", respectively. The foil's composition in Au and Cu was determined from the measured intensity ratio, by applying the XRF fundamental parameters method. Specifically, the XMI-MSIM simulation code [39,40] was executed, using as input the X-ray excitation spectrum, the spectrometer's geometry, and the detector's characteristics of the M6 spectrometer. For gilding thickness in the range of 0.1–1.0 μm (which is the typical thickness range for post-Byzantine gold leaves, [19]), the extracted Au weight composition is about 92% *w/w*; therefore, it is deduced that the gilding was performed by using high-purity gold leaves.

It shall be noted that the gold leaves do not interfere considerably with the painted areas, and this indicates that the painter cut the leaves taking care to fit as precisely as possible the areas to be gilded in order to reduce the consumption of this costly painting material. Moreover, it is observed that the maximum width of the leaves reaches about 5.4 cm (see the arrow on the Au map, Figure 4); therefore, it is assumed that the leaves used deviate substantially from the European medieval and Greek Byzantine equivalents. The latter were mostly distributed in the form of rectangle leaves with sides measuring between 6.0 and 7.5 cm [41,42]. Additionally, recent research on a considerable corpus of Greek icons has highlighted the existence of several Greek, late post-Byzantine (i.e., from 18th c. onwards) icons that bear rather small (in terms of surface area) gold leaves too [43], therefore, the finding of the current study corroborates the assumption that the Au-leaves' size was gradually reduced during the period in consideration. It is worth noting that the gold leaves used by post-Byzantine painters were extremely thin; their thickness has been found to be in the range of 0.1 to 1.0 μm [19,44]. Additionally, it is interesting to comment on the traces of Au that are spotted in the waist of St John, where gilding seems irrelevant at first sight. The circular shape of these Au-remnants, along with the posture of Saint John's left hand and the details of the preliminary drawing revealed in this particular area (see Section 4), indicates that the original painting portrayed a circular dish bearing the head of St John at this very point, an iconographic element often seen in other representations of St John.

The Au-bearing areas show in addition Si, Ti, and Fe. These elements presumably pertain to the gold leaves' gluing agent; especially for Ti it shall be noted that it is often detected as a minor admixture in clayey poliments used as gilding substrates [19,45]. Therefore, these aforementioned elements indicate the employment of a fine iron-rich clayey material, probably a bole-like substance [19,46], which upon stereoscopic investigation turned out to be of a rather yellowish-orangish tint (Figure 7a). Indeed, according to the traditional post-Byzantine painting techniques, the background/campus gold leaves were almost always applied on red or yellow clayey substrates/poliments that were covering the bare gesso grounds [19,20]. Finally, it is worth noting that, in the gilded areas, the poliment-related elements Fe, Ti, and Si expand beyond gold-covered areas (Figures 4 and 7a), highlighting thus the fragility of the extremely thin gold leaves (see above) that are very easily worn-out upon careless treatment of gilded surfaces.

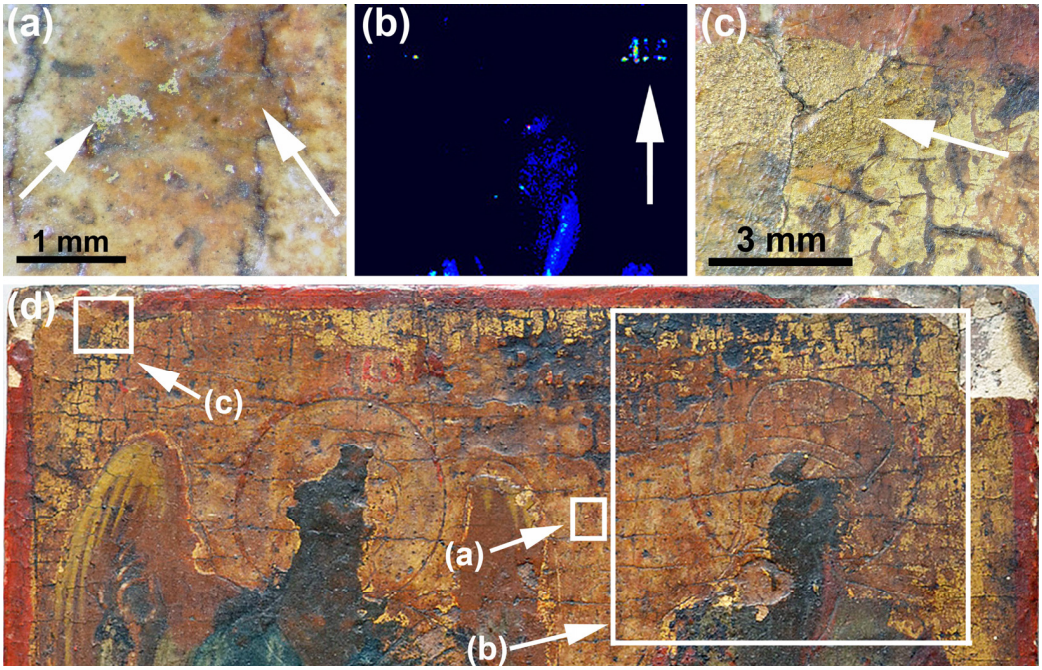

Figure 7. (**a**) detail of the yellow-orange poliment (right arrow) and remnants of original gold leaf (left arrow) (stereoscope, 40×). (**b**): detail of the mercury distribution map (Hg/Lα, Figure 7) showing original lettering above the Hierarch (arrow). (**c**): bronze powder (arrow) covering original gilding, upper left corner of the icon (stereoscope, 16×). (**d**): detail of the upper part of the studied icon where the areas that correspond to Figure 6a–c are marked.

3.2.3. The Paint Layers

Apart from the gilded areas where the detected Fe is due to the presence of the gold leaves' gluing agent/poliment (bole), Fe is also detected in the yellow-colored wings of St. John, the flesh parts, the remnants of St John's greenish vestment and on the olive-green ground (Fe map, Figure 4). In the case of the wings, the high Fe hints towards the employment of yellow ochre, yet these areas show Mn too; hence, the pigment should be rather characterized as sienna-type ochre [46,47]. Mn accompanies Fe in the dark-colored flesh areas, too; therefore, an umber brown earth pigment is deduced for rendering these areas [46,47]. Finally, the Fe detected in the greenish areas indicates the use of green earth, as the pertinent pigments are known to contain considerable iron (often in the range between 15 wt% and 25 wt%, [26]).

Pb shows high intensity in all the representations of flesh (especially on highlights), in the off-white/whitish lower part of St John's wings and on his inner bluish vestment, as well as on the Hierarch's pallium (Figure 6), suggesting the extensive use of lead white [48]. Significant Pb is also detected in many other (non-whitish) areas, such as in the greenish ground and the bright red vestment of the Hierarch, and this indicates that lead-based pigments (presumably lead white and minium) were intermixed with other pigments to render specific hues in this painting [49]; besides, the mixing of various pigments was very frequently practiced by post-byzantine painters [20]. However, of particular interest is the detection of Pb on the yellowish highlights of St John's wings, where Sb is also detected (Figure 2), thus indicating the employment of lead-antimony (or Naples) yellow [49]. This possibility is fascinating, as Naples yellow has rarely been identified in Greek icons [27].

On the other hand, Hg shows high intensity on the Hierarch's red vestment and the red margin line on the periphery of the painting (Figure 6), reflecting the employment of mercury sulfide/vermilion [27,47,50]. Minor Hg is also detected on flesh parts; indeed, a bit of vermilion was customarily intermixed with pigments used to render flesh midtones in order to impart a warm tint [20]. Most importantly, the elemental distribution map of Hg (vermilion) revealed that on the upper part of the painting, there exist remnants of an

inscription that are currently invisible to the naked eye (Figure 7b). Three letters appearing above and on the right of the Hierarch's head read ANΔ or AIΔ and might be used as a hint for identifying the name of the unknown Hierarch.

Interestingly, a small part of an inscription with the Greek letters "ιωA" (standing for Ιωάννης-Ioannis/John) appears just above the head of St John the Forerunner in the elemental distribution map of Zn (Figure 6); in addition, Zn is detected on the red margins of the painting, on the Saints' haloes outlines and on scattered spots on the Hierarch's red vestment (Figure 7). The fact that the Zn-based red margin covers the later re-gessoing on the bottom of the painting (see Section 3.2.1 and Figures 4 and 6) clearly indicates that the Zn-rich areas pertain to later retouching interventions that compensated for losses on the red pictorial elements such as the margin, the red vestment, the inscription, etc. It is worth noting that Zn may not be directly related to a specific red pigment, yet it might reflect the presence of zinc white (ZnO) [47,51]. This substance was often intermixed with various synthetic organic pigments and occasionally used as a substrate for manufacturing red and other lake pigments.

Additionally, some of the Zn-bearing spots also show intense Ba (Figure 6). Therefore, the use of lithopone in these areas is inferred. Lithopone, a mixture of barium sulfate ($BaSO_4$) and zinc sulfide (ZnS), started circulating among painters after 1874 AD [52], hence its detection gives a terminus post quem for the execution of the retouching intervention on the Hierarch's vestment. Nevertheless, Ba elemental peaks (not accompanied by Zn) show considerable intensity all over the aforementioned red vestment, and this indicates that a pigment (presumably red lake) containing $BaSO_4$ as a filler or substrate [47,53] was applied in this area. In fact, it has been well documented that post-Byzantine painters often used red lakes to impart specific hues when rendering red vestments (see, e.g., [27,54]).

Moreover, areas containing Cr and Cu appear scattered over the recto of the icon (Figure 6). In particular, high-intensity Cr peaks appear in the spectra collected from the upper left corner, the re-gessoing at the bottom, and in various spots all over the painting (green, yellow, and red spots in Figure 6, Cr map); in all these cases, Cr is accompanied by Ba (Figure 6). As the Cr-Ba spots abound on the surface of the calcium carbonate re-gessoing material, it is inferred that these elements shall be attributed to a pigment mixture used in the frame of a later intervention. On the contrary, traces of Cr are detected in other areas of the original painting (pale blue areas in Figure 6, Cr map), particularly in the yellow highlights of St John's wings, on the cover of the book held by the Hierarch and in the greenish ground; considering that these areas show the characteristic presence of Sb (Figure 2) as well as high Pb, it is assumed that Cr reflects employment of the yellow lead chromate pigment ($PbCrO_4$). This pigment was first synthesized around 1800 AD, just after the discovery of Cr by the French chemist Louis Nicholas Vauquelin in 1797 AD [55], and a recent study has shown that it was very soon adopted in a rather large scale by Greek icon painters [29].

Finally, the MA-XRF investigation of the painting revealed that a small area on the upper left corner of the icon and a few spots on the vestment of the Hierarch and elsewhere show high Cu along with Zn (Figure 6). In all these cases, the Cu/Zn-rich phases appear on areas that were initially gilded, while through stereoscopic inspection, they were found to show a characteristic flake-like appearance (Figure 7c). Therefore, it is concluded that these areas correspond to later retouching interventions executed in order to compensate for losses of the gilding. Besides, bronze powders (and leaves) were often used from the 19th century onwards for retouching decayed gilded areas or producing low-cost gilding imitations [27,56].

3.3. The Verso of the Icon (Wooden Panel)

The MA-XRF investigation of the verso of the icon yielded interesting data that reveal much information about the history of the painting. The elemental distribution map of Ca (Figure 8) highlights the existence of multiple later interventions that aimed at filling voids in the wooden support. The use of gypsum plus skin glue filler for the treatment of decayed

wooden supports is described in the early 18th century "Hermeneia of the art of painting", the renowned textbook that was compiled by the hieromonk and icon painter Dionysius of Fourna [20,28]. In the case of the icon in consideration, the detected Ca (that highlights the presence of fillers) shows a correlation with S (Figure 8) indicating thus the employment of gypsum. Nevertheless, Zn and Ba accompany Ca in some of these areas and this suggests the use of a mixed filler (presumably gypsum or chalk mixed with lithopone) in these cases.

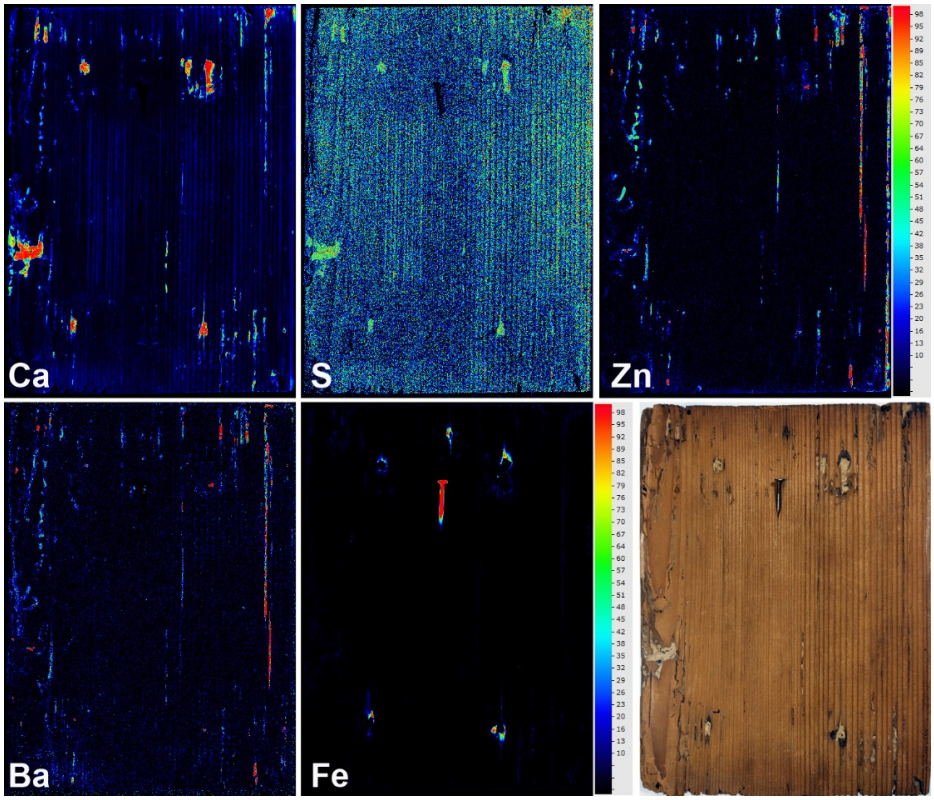

Figure 8. From upper left to bottom right: elemental distribution maps of Ca (Kα), S (Kα), Zn (Kα), Ba (Lα), and Fe (Kα) and a photograph of the verso of the icon.

Of particular interest is the distribution of Fe on the verso of the painting. The relevant MA-XRF elemental distribution map is dominated by the presence of a nail that was probably attached for hanging purposes (Figure 8). However, there appear five other Fe-rich spots on the back of the icon, three laying over the nail and two laying close to the bottom of the icon. The uppermost Fe-bearing spot (just above the nail in Figure 8) most probably pertains to an older hanging nail replaced by the current one. On the contrary, the other four spots coincide with areas where the Ca-S filler has been applied, and this indicates that they correspond to nails that were at some time removed, and then their holes were treated with a filler. Given the symmetrical placement of these four spots and their position in pairs on the upper and bottom parts of the icon, it is inferred that they correspond to the nails used to attach a pair of cross-bars on the back of the icon. Besides, cross-bars are often found in panel paintings and sometimes need to be removed in the framework of conservation interventions to preserve the wooden panel [57].

Finally, the investigation of the current icon through X-ray radiography (XRR) yielded-even after proper digital photographic processing of the relevant file—an image of relatively low contrast due to the presence of the partially inserted on the back of the icon iron nail (Figure 9 left). This metallic element acts as the major obstacle on the X-rays pathway and, hence, appears as the area of maximum brightness, minimizing thus the potentiality to discriminate subtle contrast differences between the various pictorial elements. Moreover,

the dense iron nail reacts with the incoming X-ray beam, acting as a secondary radiation source that considerably obscures its surroundings (Figure 9 left).

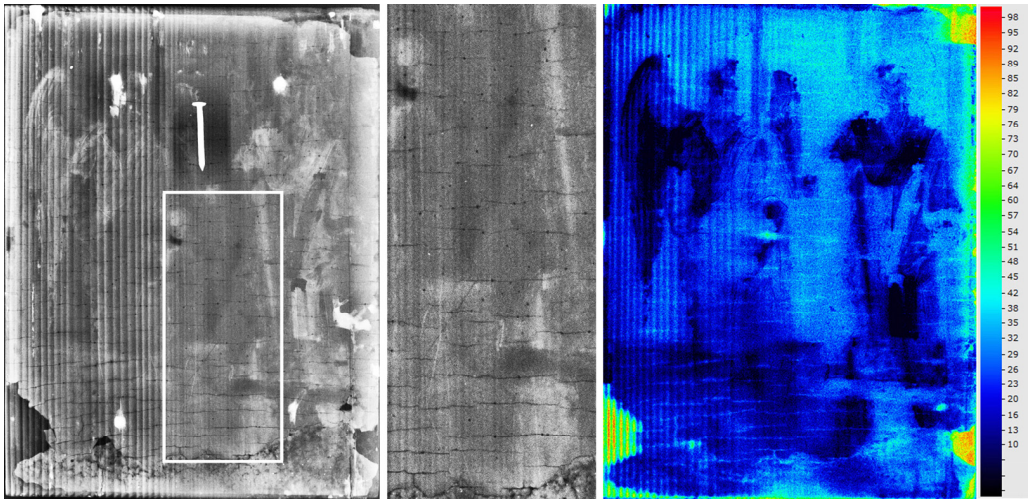

Figure 9. (**Left**) XRR of the icon under investigation; rectangle indicates the detail shown in middle. Middle: XRR detail from the area between the two figures showing tenths of pinholes. (**Right**) Compton scattering intensity distribution map, recto of the icon.

4. Discussion

The MA-XRF analysis allowed for the identification of the materials and techniques used in the original painting: a calcium sulfate ground received a painting executed in lead white, vermilion, umber, and sienna-type ochres, possibly Naples yellow, lead chromate, green earth, a red (?) organic lake, and gold leaves, while the employment of indigo blue pigment is inferred (no detection of any characteristic elements such as Fe, Cu, Co, etc. in the bluish vestment of St John). As for the latter, it is mentioned that it is regarded as the most widely used blue pigment in the framework of post-Byzantine Greek painting [26]. The inclusion of lead chromate in the original palette of the painting verifies the stylistic dating of the artifact to the early 19th century.

Moreover, based on the MA-XRF analysis results, it is obvious that the item in consideration has received interventions for purpose of compensating for extensive paint and gesso losses. In particular, the notable gesso loss on the bottom of the item has been filled by using a Ca-based filler (Figure 4). At the same time, the various gaps on the verso of the icon (wooden panel) were treated by using two distinct materials, namely a calcium sulfate compound and a mixed filler containing Ca, Ba, and Zn compounds (see Figure 8 and Section 3.3). Note that the employment of two fillers in the back of the icon clearly indicates that the item has received at least two distinct restoration interventions. On the other side of the panel (recto), the analysis revealed that a Zn-bearing red pigment had been used for retouching losses on the bright red areas (Figure 6), and a few losses of the gilding have been treated by using brass powder. At the same time, the use of yellow lead chromate for retouching purposes is also documented by the MA-XRF data (see Figure 6 and Section 3.2.3). Based on the identified pigments and fillers, it is inferred that at least some interventions were executed after 1874 AD when lithopone was first produced on a large scale.

As for the XRR, it has already been mentioned that the dense iron nail that is inserted on the back of the icon is the major obstacle of the X-ray beam and reacts with the latter creating secondary radiation that negatively affects the quality of the acquired radiograph (Figure 9 left). Therefore, not much information regarding the painting materials and techniques of the icon could be gained through XRR in this case. Nevertheless, the radiograph reveals indeed one particularly interesting detail that is not clearly visible on the MA-XRF elemental distribution maps: throughout the surface of the painting there do exist tens

of small pinholes that mostly pierce through cracks of the gesso (Figure 9 middle). These holes were probably generated during a past consolidation intervention that employed the injection of a liquid consolidant through the gesso cracks; such interventions were indeed once practiced, and their detrimental side effects are occasionally spotted in paintings [58]. Moreover, XRR pictures the grain of the wooden support very clearly, which shows a gradually changing texture from left to right since the panel is part of a tangential cut (see also Figure 3 BW vs. multicolor maps). Note that the wood grain appears in the MA-XRF map that demonstrates changes in the intensity of Compton scatter, as the latter is partially affected by the composition of the analyte (and, hence, the wood grain) (Figure 9 right). In particular, the Compton intensity is inversely proportional to the total mass absorption coefficient [59], which is the sum of the incoming primary beam mass absorption coefficient for the Rh Kα photons (20.2 keV) and the Compton Rh Kα scattered photons (18.8 keV). The mass absorption coefficient is an increasing function of the atomic number of the elements that the primary and scattered radiation encounters in its path [36]. Consequently, the Compton intensity decreases as the mean atomic number of the irradiated area increases. This explains the low Compton intensity in the regions of high Z elements, like Pb- and Hg-based pigments. Conversely, the maximum Compton intensity is observed in areas where pigment layers have been removed, while the preparatory layer is either thin or absent. Consequently, the study of the Rh Kα Compton intensity distribution per pixel provides complementary information to the XRR method. Compton allows single-side mapping of the mean atomic number distribution at the same time as the elemental mapping measurement. As XRR requires access on both sides of the painting [12], the Compton intensity mapping is an exciting alternative in case this is not feasible.

Finally, it is worth highlighting the potential to track the incised preparatory drawing of the painting. Although the drawing does not show up clearly in the XRR for the reasons mentioned above, it does appear in many of the MA-XRF elemental distribution maps (Figure 10). For instance, in the case of the calcium map, the drawing is very clearly seen in areas where bare or almost bare gesso exists simply because the incised lines are in fact areas where less Ca is detected; this is graphically demonstrated in the waist of St John where the incised facial characteristics of the head on the dish appear (see also the relevant discussion about Au in Section 3.2.2). Further details of the preliminary drawing show up in other elemental distribution maps, two characteristic examples being the maps of Fe and Pb shown in Figure 10. In both these cases, relevant pigments (ochre and lead white) have settled within the incision of the drawing resulting thus in higher elemental peak intensities on the corresponding MA-XRF maps. Therefore, it is inferred that, through the examination of multiple MA-XRF maps, it is possible to gain a complete and thorough view of the preliminary/preparatory drawing as well, a possibility that does not however reduce the importance of other techniques (e.g., infrared reflectography) able to reveal preliminary drawings [60].

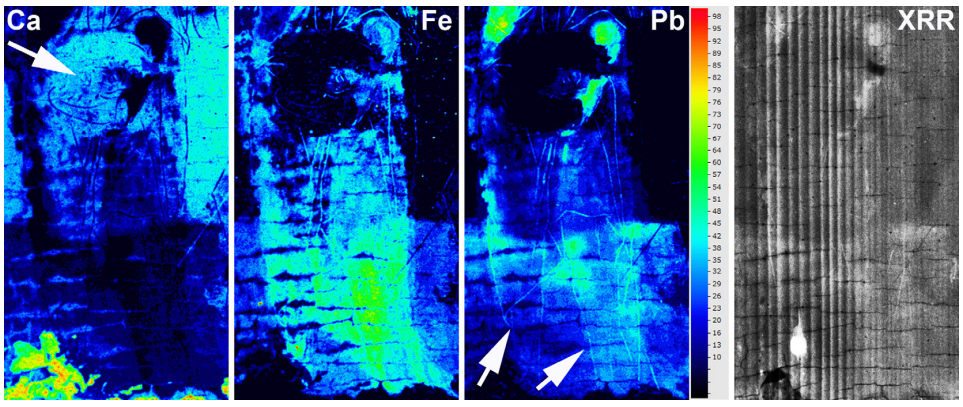

Figure 10. From left to right: elemental distribution maps of Ca (Kα), Fe (Kα), and Pb (Lα), and XRR of the lower part of St John's body. Arrows highlight details of the preliminary incised drawing.

5. Conclusions

A thorough examination of the complex MA-XRF data collected from the analysis of a heavily altered post-Byzantine Greek icon led to the identification of the original painting materials and techniques and the discrimination of at least two distinct later interventions. The inclusion of lead chromate in the original palette corroborates the stylistic dating of the icon to the early 19th century. At the same time, the identification of lithopone-base substances in later interventions suggests that some were executed after 1874 AD. Significant findings include the spotting of remnants of an original inscription and the tracing of the preparatory drawing, while the MA-XRF data indicate the possible use of Naples yellow, a pigment rarely identified in Greek icons. Additionally, XRR indeed provided interesting results, yet it is demonstrated that it can by no means stand alone as an analytical tool for identifying easel painting with complex restoration history as the one in consideration. Moreover, we have demonstrated that the Compton scattering provides complementary information to the XRR method, allowing single-side mapping of the mean atomic number distribution. Finally, the fact that the weak Sb intensity was hard to be determined upon data processing suggests that the scholars dealing with the MA-XRF investigation of paintings should scrutinize the pertinent data before proceeding to the creation of elemental distribution maps.

Author Contributions: Conceptualization, G.P.M. and D.F.A.; methodology, D.F.A., A.A. and G.P.M.; software, A.A. and T.G.; validation, G.P.M. and D.F.A.; formal analysis, A.A. and T.G.; investigation, G.P.M., D.F.A., A.A., and T.G.; resources, D.F.A. and G.P.M.; data curation, A.A. and T.G.; writing—original draft preparation, G.P.M.; writing—review and editing, D.F.A. and G.P.M.; visualization, G.P.M., D.F.A., and A.A.; supervision, D.F.A. and G.P.M.; project administration, D.F.A.; funding acquisition, D.F.A. All authors have read and agreed to the published version of the manuscript.

Funding: We acknowledge the support of this work by the project "Center for research, Quality analysis of cultural heritage materials and communication of science" (MIS 5047233) which is implemented under the Action "Reinforcement of the Research and Innovation Infrastructure", funded by the Operational Programme "Competitiveness, Entrepreneurship and Innovation" (NSRF 2014-2020) and co-financed by Greece and the European Union (European Regional Development Fund).

Institutional Review Board Statement: Not applicable.

Informed Consent Statement: Not applicable.

Data Availability Statement: Not applicable.

Acknowledgments: Special thanks are due to Yannis Bassiakos and Eleni (Liana) Filippaki from INN, NCSR "Demokritos" for providing access to the milliprobe XRF setup. Georgios Sboukis, head of a Medical Imaging private center, is sincerely acknowledged for offering the possibility to examine through digital radiography the icon. Also, the personnel of the Department of Conservation of Antiquities and Works of Art, West Attica University, is sincerely acknowledged for providing access to laboratory equipment. Finally, the authors warmly thank the four anonymous reviewers who, by providing thoughtful and constructive comments, contributed significantly to improving the quality of the current article.

Conflicts of Interest: The authors declare no conflict of interest.

References

1. Mantler, M.; Schreiner, M. X-ray fluorescence spectrometry in art and archaeology. *X-ray Spectrom.* **2000**, *29*, 3–17. [CrossRef]
2. Thompson, G. Penetration of radiation into old paint films. *Natl. Gallery Tech. Bull.* **1979**, *3*, 25–33.
3. Janssens, K.; Van der Snickt, G.; Vanmeert, F.; Legrand, S.; Nuyts, G.; Alfeld, M.; Monico, L.; Anaf, W.; De Nolf, W.; Vermeulen, M.; et al. Non-Invasive and Non-Destructive Examination of Artistic Pigments, Paints, and Paintings by Means of X-Ray Methods. *Top. Curr. Chem.* **2016**, *374*, 1–52. [CrossRef]

4. Romano, F.P.; Caliri, C.; Nicotra, P.; Di Martino, S.; Pappalardo, L.; Rizzo, F.; Santos, H.C. Real-time elemental imaging of large dimension paintings with a novel mobile macro X-ray fluorescence (MA-XRF) scanning technique. *J. Anal. At. Spectrom.* **2017**, *32*, 773–781. [CrossRef]
5. Van der Snickt, G.; Legrand, S.; Slama, I.; Van Zuien, E.; Gruber, G.; Van der Stighelen, K.; Klaassen, L.; Oberthaler, E.; Janssens, K. In situ macro X-ray fluorescence (MA-XRF) scanning as a non-invasive tool to probe for subsurface modifications in paintings by P.P. Rubens. *Microchem. J.* **2018**, *138*, 238–245. [CrossRef]
6. Walczak, M.; Tarsińska-Petruk, D.; Płotek, M.; Goryl, M.; Kruk, M.P. MA-XRF study of 15th–17th century icons from the collection of the National Museum in Krakow, Poland. *X-Ray Spectrom.* **2019**, *48*, 303–310. [CrossRef]
7. Kokiasmenou, E.; Caliri, C.; Kantarelou, V.; Karydas, G.A.; Romano, F.P.; Brecoulaki, H. Macroscopic XRF imaging in unravelling polychromy on Mycenaean wall-paintings from the Palace of Nestor at Pylos. *J. Archaeol. Sci. Rep.* **2020**, *29*, 102079. [CrossRef]
8. Alfeld, M.; Mösl, K.; Reiche, I. Sunset and moonshine: Variable blue and yellow pigments used by Caspar David Friedrich in different creative periods revealed by in situ XRF imaging. *X-ray Spectrom.* **2021**, *50*, 341–350. [CrossRef]
9. Mazzinghi, A.; Ruberto, C.; Castelli, L.; Czelusniak, C.; Giuntini, L.; Mandò, P.A.; Taccetti, F. MA-XRF for the Characterisation of the Painting Materials and Technique of the Entombment of Christ by Rogier van der Weyden. *Appl. Sci.* **2021**, *11*, 6151. [CrossRef]
10. Janssens, K.; Dik, J.; Cotte, M.; Susini, J. Photon-based techniques for nondestructive subsurface analysis of painted cultural heritage artifacts. *Acc. Chem. Res.* **2010**, *43*, 814–825. [CrossRef]
11. Ghigo, T.; Bone, D.; Howell, D.; Domoney, K.; Gironda, M.; Beedy, A. Material Characterisation of William Burges' *Great Bookcase* within the Disruption of a Global Pandemic. *Stud. Conserv.* **2022**, 1–16. [CrossRef]
12. Alfeld, M.; Broekaert, J.A.C. Mobile depth profiling and sub-surface imaging techniques for historical paintings—A review. *Spectrochim. Acta Part B At. Spectrosc.* **2013**, *88*, 211–230. [CrossRef]
13. Lizun, D.; Kurkiewicz, T.; Szczupak, B. Exploring liu kang's paris practice (1929–1932): Insight into painting materials and technique. *Heritage* **2021**, *4*, 828–863. [CrossRef]
14. Martins, A.; Davis, E.; Kwartler, T. Max Ernst's woman, old man, and flower (1923–1924): Four paintings in one revealed by technical imaging. *Heritage* **2021**, *4*, 2224–2236. [CrossRef]
15. Miguel, C.; Bottura-Scardina, S.; Bottaini, C.; Valadas, S.; Candeias, A.; Bilou, F. The Power of Combining MA-XRF, Infrared Reflectography and Digital Microscopy to Unveil the Production of the 16th Century Illuminated Charter of Évora: What May Be Hidden under a Painted Surface? *Heritage* **2022**, *5*, 286–296. [CrossRef]
16. Gerodimos, T.; Asvestas, A.; Mastrotheodoros, G.P.; Chantas, G.; Liougos, I.; Likas, A.; Anagnostopoulos, D.F. Scanning X-ray Fluorescence Data Analysis for the Identification of Byzantine Icons' Materials, Techniques, and State of Preservation: A Case Study. *J. Imaging* **2022**, *8*, 147. [CrossRef]
17. Sotiropoulou, S.; Daniilia, S. Materials aspects of icons. A review on physicochemical studies of Greek icons. *Acc. Chem. Res.* **2010**, *43*, 877–887. [CrossRef]
18. Mastrotheodoros, G.P.; Beltsios, K.G.; Bassiakos, Y.; Papadopoulou, V. On the Grounds of Post-Byzantine Greek Icons. *Archaeometry* **2016**, *58*, 830–847. [CrossRef]
19. Mastrotheodoros, G.P.; Beltsios, K.G.; Bassiakos, Y.; Papadopoulou, V. On the Metal-Leaf Decorations of Post-Byzantine Greek Icons. *Archaeometry* **2018**, *60*, 269–289. [CrossRef]
20. Dionysios; Hetherington, P. *Dionysius of Fourna, The 'Painter's Manual' of Dionysius of Fourna*; Hetherington, P., Translator; Oakwood Publications: Torrans, CA, USA, 1996.
21. Βοκοτόπουλος, Π. *Βυζαντινές Εικόνες [Byzantine Icons]*; Ekdotike Athenon: Athens, Greece, 1995.
22. Newman, N.; Harrison, L.; Thomas, D.; Dyer, J.; Taylor, J. The study and conservation of four ancient Egyptian funerary portraits: Provenance, conservation history and structural treatment. *Br. Mus. Tech. Res. Bull.* **2013**, *7*, 1–14.
23. Κόρδης, Γ. *Οι προσωπογραφίες του Φαγιούμ και η βυζαντινή εικόνα [The Fayum Portraits and the Byzantine Icon]*; Armos Publications: Athens, Greece, 2001.
24. Evseeva, L.M. *A History of Icon Painting: Sources, Traditions, Present Day*; Evseeva, L.M., Ed.; Cook, K., Translator; Grand-Holding Publishers: Moscow, Russia, 2007.
25. Χατζηδάκης, Μ. *Έλληνες ζωγράφοι μετά την Άλωση (1450–1830) [Greek Painters after the Fall of Constantinople (1450–1830)]*; Center for Neo-Hellenic Studies: Athens, Greece, 1987.
26. Mastrotheodoros, G.P.; Beltsios, K.G.; Bassiakos, Y. On the blue and green pigments of post-byzantine Greek icons. *Archaeometry* **2020**, *62*, 774–795. [CrossRef]
27. Mastrotheodoros, G.P.; Beltsios, K.G.; Bassiakos, Y. On the red and yellow pigments of post-byzantine Greek icons. *Archaeometry* **2021**, *63*, 753–778. [CrossRef]
28. Mastrotheodoros, G.P.; Beltsios, K.G. Sound practice and practical conservation recipes as described in Greek post-byzantine painters' manuals. *Stud. Conserv. Stud. Conserv.* **2019**, *64*, 42–53. [CrossRef]
29. Serafima, S.; Duliu, O.G.; Manea, M.M.; Vasilica, S.; Radulescu, C.; Constantinescu, B.; Stan, D.; Culicov, O.-A.; Zincovscaia, I. Complex investigation of the five 19th century Russian-Lipovan icons. *Microchem. J.* **2019**, *150*, 104126. [CrossRef]

30. Klisińska-Kopacz, A.; Obarzanowski, M.; Frączek, P.; Moskal-del Hoyo, M.; Gargano, M.; Goslar, T.; Chmielewski, F.; Dudała, J.; del Hoyo-Meléndez, J.M. An analytical investigation of a wooden panel painting attributed to the workshop of Lucas Cranach the Elder. *J. Cult. Herit.* **2022**, *55*, 185–194. [CrossRef]
31. Βοκοτόπουλος, Π. *Εικόνες της Κέρκυρας [Icons of Corfu]*; National Bank of Greece Cultural Foundation: Athens, Greece, 1990.
32. Βασιλάκη, Μ. *Οι Εικόνες του Αρχοντικού Τοσίτσα. Η Συλλογή του Ευάγγελου Αβέρωφ [The Icons of the Tositsa Mansion. The Collection of Evangelos Averof]*; Baron Michael Tossizza Foundation: Athens, Greece, 2012.
33. Chatzidakis, M.; Djurić, V.; Lazović, M. *Les Icons Dans les Collections Suisses*; Benteli Publications: Berne, Switzerland, 1968.
34. Borboudakis, M. (Ed.) *Εικόνες Της Κρητικής Τέχνης [Icons of the Cretan Art]*; Vikelaia Library and Editions of the University of Crete: Heraklion, Greece, 1993.
35. Wolff, T.; Tagle, R.; Reinhardt, F.; Waldschlägerand, U.; Schwager, T. On the Interaction of X-rays and Samples by Quantification of Energy Deposition. In Proceedings of the Oral presentation in "European Conference on X-ray Spectrometry 2022"/EXRS-2022, Bruges, Belgium, 26 June–1 July 2022.
36. NIST XCOM. Photon Cross Sections Database. Available online: http:/physics.nist.gov/xcom (accessed on 20 January 2023).
37. Genestar, C. Characterization of grounds used in canvas and sculpture. *Mater. Lett.* **2002**, *54*, 382–388. [CrossRef]
38. Franceschi, E.; Locardi, F. Strontium, a new marker of the origin of gypsum in cultural heritage? *J. Cult. Herit.* **2014**, *15*, 522–527. [CrossRef]
39. Brunetti, A.; Golosio, B.; Schoonjans, T.; Oliva, P. Use of Monte Carlo simulations for cultural heritage X-ray fluorescence analysis. *Spectrochim. Acta Part B At. Spectrosc.* **2015**, *108*, 15–20. [CrossRef]
40. Schoonjans, T.; Solé, V.A.; Vincze, L.; Sanchez del Rio, M.; Appel, K.; Ferrero, C. A general Monte Carlo simulation of energy-dispersive X-ray fluorescence spectrometers—Part 6. Quantification through iterative simulations. *Spectrochim. Acta Part B At. Spectrosc.* **2013**, *82*, 36–41. [CrossRef]
41. Bomford, D.; Dunkerton, J.; Gordon, D.; Roy, A. *Art in the Making: Italian Painting before 1400*; National Gallery: London, UK, 1990.
42. Milanou, K.; Vourvopoulou, C.; Vranopoulou, L.; Kalliga, A. Angelo's Painting Technique: A description of panel painting construction, materials and painting method based on a study of seven signed icons. In *Icons by the Hand of Angelos*; Benaki Museum: Athens, Greece, 2008; pp. 19–113.
43. Μαστροθεόδωρος, Γ.Π. Χρωστικές Κονίες και άλλα Υλικά Μεταβυζαντινή Ζωγραφικής [Pigments and Other Materials of Post-Byzantine Painting]. Ph.D. Thesis, University of Ioannina, Ioannina, Greece, 2016.
44. Mastrotheodoros, G.P.; Anagnostopoulos, D.F.; Filippaki, E.; Beltsios, K.G.; Bassiakos, Y. Probing the birthplace of the "Epirus/NW Greece School" of painting: Analytical investigation of the Filanthropinon monastery murals. Part II: Non-pigment materials and painting technique. *Archaeol. Anthropol. Sci.* **2019**, *11*, 5781–5798. [CrossRef]
45. Grygar, T.; Hradilová, J.; Hradil, D.; Bezdička, P.; Bakardjieva, S. Analysis of earthy pigments in grounds of Baroque paintings. *Anal. Bioanal. Chem.* **2003**, *375*, 1154–1160. [CrossRef] [PubMed]
46. Mastrotheodoros, G.P.; Beltsios, K.G. Pigments—Iron-based red, yellow, and brown ochres. *Archaeol. Anthropol. Sci.* **2022**, *14*, 35. [CrossRef]
47. Eastaugh, N.; Walsh, V.; Chaplin, T.; Siddall, R. *Pigment Compendium: A Dictionary and Optical Microscopy of Historical Pigments*; Butterworth-Heinemann: London, UK, 2008.
48. Gettens, R.J.; Kühn, H.; Chase, W.T. Lead white. In *Artist's Pigments: A Handbook of Their History and Characteristics*; Roy, A., Ed.; National Gallery of Art: Washington, DC, USA, 1993; Volume 2, pp. 67–82.
49. Gliozzo, E.; Ionescu, C. Pigments—Lead-based whites, reds, yellows and oranges and their alteration phases. *Archaeol. Anthropol. Sci.* **2022**, *14*, 17. [CrossRef]
50. Mastrotheodoros, G.P.; Beltsios, K.G. Recipes for pigment manufacturing in Greek post-byzantine painting manuals. *Sci. Cult.* **2022**, *8*, 147–159. [CrossRef]
51. Kühn, H. Zinc white. In *Artist's Pigments: A Handbook of Their History and Characteristics*; Feller, R.L., Ed.; National Gallery of Art; Cambridge University Press: Cambridge, UK, 1986; pp. 169–186.
52. Feller, R.L. Barium Sulfate—Natural and Synthetic. In *Artist's Pigments: A Handbook of Their History and Characteristics*; Feller, R.L., Ed.; National Gallery of Art; Cambridge University Press: Cambridge, UK, 1986; pp. 47–64.
53. Gabrieli, F.; Doherty, B.; Miliani, C.; Degano, I.; Modugno, F.; Uldank, D.; Kunzelman, D.; Buzzegoli, E.; Pattie, M.; Rosi, F. Micro-Raman and SER spectroscopy to unfold Lefranc's early organic pigment formulations. *J. Raman Spectrosc.* **2016**, *47*, 1505–1513. [CrossRef]
54. Karapanagiotis, I.; Minopoulou, E.; Valianou, L.; Daniilia, S.; Chryssoulakis, Y. Investigation of the colourants used in icons of the Cretan School of iconography. *Anal. Chim. Acta* **2009**, *647*, 231–242. [CrossRef]
55. Kühn, H.; Curran, M. Chrome Yellow and Other Chromate Pigments. In *Artist's Pigments: A Handbook of Their History and Characteristics*; Feller, R.L., Ed.; National Gallery of Art; Cambridge University Press: Cambridge, UK, 1986; pp. 186–217.
56. Gulotta, D.; Goidanich, S.; Bertoldi, M.; Bortolotto, S.; Toniolo, L. Gildings and false gildings of the baroque age: Characterization and conservation problems. *Archaeometry* **2012**, *54*, 940–954. [CrossRef]
57. Bisacca, G.; de la Fuente Martínez, J. The Treatment of Dürer's Adam and Eve Panels at the Prado Museum. In *Facing the Challenges of Panel Paintings Conservation: Trends, Treatments, and Training*; Phenix, A., Chui, S.A., Eds.; The Getty Conservation Institute: Los Angeles, CA, USA, 2011; pp. 10–24.
58. Knut, N. *The restoration of Paintings*; Könemann: Cologne, Germany, 1999.

59. Vrebos, B.A.R. *Compensation Methods in Quantitative Analysis, Handbook of Practical X-ray Fluorescence Analysis*; Kawahara, N., Shoji, T., Beckhoff, B., Kanngießer, B., Langhoff, N., Wedell, R., Wolff, H., Eds.; Springer: Berlin/Heidelberg, Germany, 2006; p. 364.
60. Alexopoulou, A.; Kaminari, A.A.; Moutsatsou, A. Multispectral and hyperspectral studies on Greek monuments, archaeological objects and paintings on different substrates. Achievements and limitations. *Commun. Comput. Inf. Sci.* **2019**, *962*, 443–461.